LETTERS

Quantum phase transition in a single-molecule quantum dot

Nicolas Roch[1], Serge Florens[1], Vincent Bouchiat[1], Wolfgang Wernsdorfer[1] & Franck Balestro[1]

Quantum criticality is the intriguing possibility offered by the laws of quantum mechanics when the wave function of a many-particle physical system is forced to evolve continuously between two distinct, competing ground states[1]. This phenomenon, often related to a zero-temperature magnetic phase transition, is believed to govern many of the fascinating properties of strongly correlated systems such as heavy-fermion compounds or high-temperature superconductors[1]. In contrast to bulk materials with very complex electronic structures, artificial nanoscale devices could offer a new and simpler means of understanding quantum phase transitions[2,3]. Here we demonstrate this possibility in a single-molecule quantum dot, where a gate voltage induces a crossing of two different types of electron spin state (singlet and triplet) at zero magnetic field. The quantum dot is operated in the Kondo regime, where the electron spin on the quantum dot is partially screened by metallic electrodes. This strong electronic coupling between the quantum dot and the metallic contacts provides the strong electron correlations necessary to observe quantum critical behaviour. The quantum magnetic phase transition between two different Kondo regimes is achieved by tuning gate voltages and is fundamentally different from previously observed Kondo transitions in semiconductor and nanotube quantum dots[4,5]. Our work may offer new directions in terms of control and tunability for molecular spintronics[6].

Quantum dots seem to be ideal devices in which to observe quantum phase transitions. First, such gate-tuneable artificial atoms offer a high degree of control by means of simple gate electrostatics. Second, owing to the nanometric confinement of the electrons, they display relatively high energy scales that allow the observation of interesting quantum phenomena at accessible temperatures. Finally, the coupling between the quantum dot and the electronic reservoirs (transport probes) produces tunnelling events that can fundamentally alter the discrete energy levels of the dot, changing them into complicated many-body wave functions. One well-studied situation in nanoscale devices (although not classified as a quantum transition) in which the interplay of these three effects is clear occurs when a single unpaired spin with $S = 1/2$ characterizes the ground state of the quantum dot. When conducting electrons move to and from the nanostructure, causing the tiny magnetic moment of the dot to alternate, a progressive screening of the atomic spin occurs, in complete analogy to the well-known Kondo effect in solids containing magnetic impurities[7,8].The Kondo effect in quantum dots is then observed as zero-bias conductance resonance[9,10], associated with the entangled state of electrons in the electronic reservoirs and in the dot, and displays a high degree of universality.

For quantum dots with even occupancy it is possible to tune the magnetic ground state of the dot between a spin-0 singlet and spin-1 triplet. Electronic tunnelling can then subtly affect the fate of the magnetic state of the quantum dot: when the singlet–triplet splitting is eventually brought to zero, the simple level crossing of the two spin states becomes a true zero-temperature quantum phase transition. When only one electronic fluid participates in the Kondo effect[2,3], a spin-1 quantum dot will be partially compensated, so that the full many-body ground state evolves between different entropy states, presenting singularities at the quantum critical point (Fig. 1a). Conversely, the opening of a second screening channel[11,12] will quench the remaining entropy, and the absence of obvious symmetry breaking generically leads to a transition being avoided[13,14].

Single-molecule quantum dots inserted in a nanoscale constriction present three features key to the observation of such sharp quantum phase transitions. First, owing to their asymmetric tunnelling geometry, a predominant single screening channel should be expected. Second, previous investigations have demonstrated large Kondo temperatures[15]. Third, as we discuss below, a gate-voltage dependence of the singlet–triplet gap for zero magnetic field can be introduced by means of a local gate[15] underneath the nanogap, which allows precise tuning of the magnetic levels of the quantum dot. Combining these three crucial requirements in a single experiment opens new possibilities for the precise control of spin states in molecular nanostructures. Other than in the realization of interesting quantum many-body effects in quantum dots, our results may also be relevant in understanding quantum criticality in correlated bulk materials[1].

We used the electromigration technique[16] (see Methods) to construct a single-molecule transistor, shown in Fig. 1b. Here we report on a full experimental study of transport measurements in terms of bias voltage V_b, gate voltage V_g, temperature T ($35\,\mathrm{mK} < T < 20\,\mathrm{K}$) and magnetic field B up to 8 T. Statistical evidence that transport takes place when we use a C_{60} molecule is provided in the Supplementary Information, together with several conductance characteristics obtained for different samples.

The general features of the single-molecule quantum dot are presented in Fig. 1c, which shows a large-scale, two-dimensional map of the differential conductance $\partial I/\partial V$ as a function of V_b and V_g at $T = 35\,\mathrm{mK}$ and $B = 0$. The distinct conducting and non-conducting regions are typical signatures of a single-molecule transistor[17]. We present measurements over two distinct Coulomb diamonds indicated by 'odd' and 'even' charge states. The sharp high-conductance ridge in the odd charge state at zero bias is clearly associated with the usual spin-1/2 Kondo effect[9,10]; detailed studies are reported in the Supplementary Information.

Henceforth we focus on the even charge state. The two-electron states can be described by their total spin S and spin projection m, and are denoted $|S, m\rangle$. The ground state of the system can thus be either a spin singlet $|0, 0\rangle$, with energy E_S, or a spin triplet, with energy E_T, described by the three states $|1, 1\rangle$, $|1, 0\rangle$ and $|1, -1\rangle$. These triplet states are degenerate for $B = 0$ but are split by the Zeeman effect, with an energy shift of $\Delta E_T = mg\mu_B B$ for each state $|1, m\rangle$, where g is the

[1]Institut Néel, CNRS and Université Joseph Fourier, BP 166, 38042 Grenoble cedex 9, France.

g-factor and μ_B is the Bohr magneton. Figure 1d presents a precise low-bias $\partial I/\partial V$ map of the even region inside the dotted rectangle of Fig. 1c. This clearly displays two distinct regions, which (in anticipation of our results) we associate with the singlet and triplet ground states. The possibility of gate-tuning the singlet–triplet splitting $E_T - E_S$ was demonstrated previously both for lateral quantum dots[18] and carbon nanotubes[19], and may originate in an asymmetric coupling of the molecular levels to the electrodes[20]. The magnetic states cross sharply at a critical gate voltage $V_g^c \approx 1.9$ V.

In the singlet region, a finite-bias conductance anomaly appears when V_b coincides with $E_T - E_S$; this is due to a non-equilibrium Kondo effect involving excitations into the spin-degenerate triplet. This effect was recently studied in a carbon-nanotube quantum dot in the singlet state[21] (see Supplementary Information). In the triplet region, two kinds of resonance are observed: a finite-bias $\partial I/\partial V$ anomaly, which is interpreted as a singlet–triplet non-equilibrium Kondo effect that disperses like $E_S - E_T$ in the V_g–V_b plane, and a sharp, zero-bias $\partial I/\partial V$ peak, which is related to a partially screened spin-1 Kondo effect[22], as indicated by the narrowness of the conductance peak.

To precisely identify these spin states, and justify our analysis in the framework of quantum criticality near the singlet–triplet crossing point, we present a detailed magneto-transport investigation of the even region. Owing to the high g-factor ($g \approx 2$) of C_{60} molecules, it is easy to lift the degeneracy of the triplet state for a C_{60} quantum dot using the Zeeman effect (see Supplementary Information). Figure 2b, d displays the evolution of the different conductance anomalies in the even region.

Figure 2b shows $\partial I/\partial V$ as a function of B and V_b for a constant gate voltage V_g chosen in the singlet region. A Zeeman-induced transition from the singlet state $|0,0\rangle$ to the lowest-m triplet state $|1,-1\rangle$ occurs as the magnetic field is increased (Fig. 2a), and is demonstrated by the clear level crossing in the conductance map. The splitting of the triplet is also apparent, and the various spectroscopic lines are consistent with the spin selection rules at both low and high magnetic field, where $|0,0\rangle$ and $|1,-1\rangle$ are the respective ground states.

In Fig. 2d we investigate the gate-induced singlet–triplet crossing for constant magnetic field. In the singlet region, the Zeeman-split triplet states are clearly seen as three parallel lines, and the transition lines from the ground state $|1,-1\rangle$ at higher gate voltage are in agreement with the energy levels depicted in Fig. 2c, confirming the singlet to triplet crossing inside the even Coulomb diamond. We note the absence of a large enhancement of the zero-bias conductance at the singlet–triplet crossing in Figs 1d and 2b. Such features were, however, observed in previous experiments of vertical semiconductor quantum dots[4], where a field-induced orbital effect can be used to make the non-degenerate triplet coincide with the singlet state, leading to a large Kondo enhancement of the conductance that is intimately related to the existence of two screening channels[23]. In carbon nanotubes[5], the Zeeman effect dominates over the orbital effect, so the transition involves the lowest-m triplet state only and Kondo signatures arise from a single channel, as in the case of well-balanced couplings of the two orbital states in the quantum dot to the electrodes[24]. The lack of either type of singlet–triplet Kondo effect in our data indicates that the predominant coupling is between a single screening channel and one of the two spin states of the single-molecule quantum dot, leading to a Kosterlitz–Thouless quantum phase transition at the singlet–triplet crossing, as predicted by the theory[2,3]. Although the peculiar magnetic response associated with this transition is not directly accessible in our scheme, we demonstrate that very specific characteristics of the Kosterlitz–Thouless transition can be observed in transport. The basic factor in the

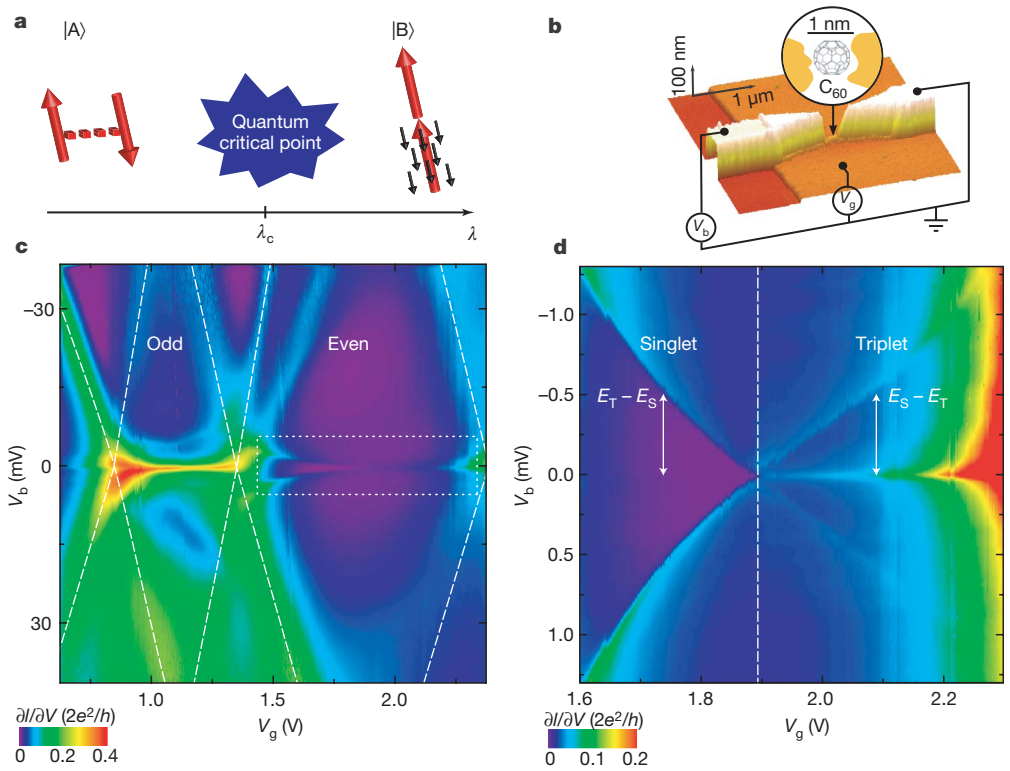

Figure 1 | Quantum phase transition, device and conductance characteristics. **a**, Quantum phase transition: a quantum state $|A\rangle$ can be driven by a non-thermal external parameter λ to another quantum state $|B\rangle$ with a different symmetry, passing through a critical point at $\lambda = \lambda_c$. In our single-molecule quantum dot device, $|A\rangle$ is a singlet state and $|B\rangle$ is a triplet state that is partially screened by one conduction electron channel, represented by black arrows. **b**, Atomic-force-microscope micrograph of the device: gold nanowire over an Al/Al_2O_3 gate, with a C_{60} molecule trapped in the nanogap formed during the electromigration. **c**, Colour map over two Coulomb diamonds of the differential conductance $\partial I/\partial V$ (in units of $2e^2/h$, where h denotes Planck's constant) as a function of bias voltage V_b and gate voltage V_g at $T = 35$ mK and $B = 0$. **d**, Detail of the differential conductance in the dotted white rectangle in **c**, showing the singlet to triplet spin transition.

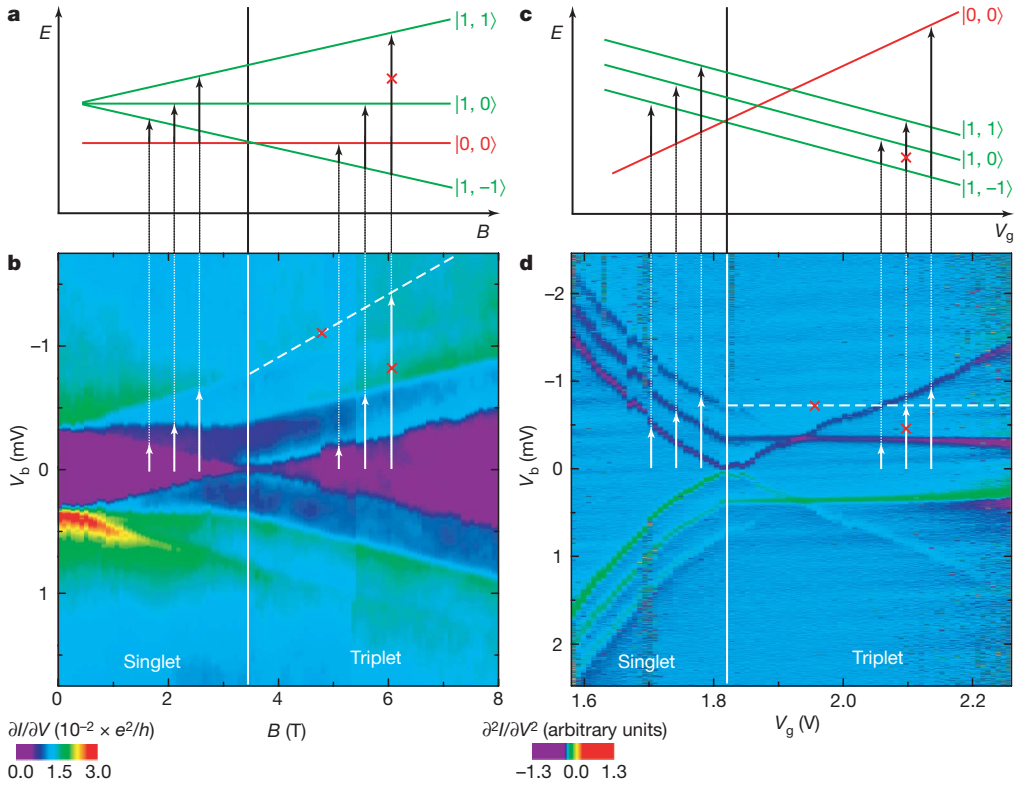

Figure 2 | Magnetic field and gate-induced singlet–triplet transition. **a**, Transition from singlet state $|0, 0\rangle$ to lowest-m triplet state $|1, -1\rangle$ induced by the Zeeman effect. **b**, $\partial I/\partial V$ measurements as a function of B and V_b at fixed gate voltage and temperature $T = 35$ mK. The crossed-out dashed line and arrow indicate that second-order spin-flip processes with $\Delta m = 2$ are not observed; see also **a**. **c**, Transition from singlet state $|0, 0\rangle$ to lowest-m triplet state $|1, -1\rangle$ induced by the gate voltage at constant magnetic field. **d**, $\partial^2 I/\partial V^2$ measurements as a function of V_g and V_b for fixed magnetic field $B = 3$ T and temperature $T = 35$ mK. The crossed-out line and arrow indicate the same thing as in **b**; see also **c**. Owing to lower contrast in the triplet region, we plot $\partial^2 I/\partial V^2$ here to improve the visibility of the data.

following discussion is that the singlet and triplet states fully dissociate into two independent spin-1/2 units near the Kosterlitz–Thouless transition, undergoing distinct Kondo screening processes.

Figure 3b shows the conductance map for gate voltages close to the critical value V_g^c, where singlet and triplet states are tuned to coincide for $B = 0$. We notice that a sharp conductance dip forms on the singlet side of the transition, in contrast to the shallow minima observed in previous experiments for two-level quantum dots in the singlet regime[18,19,25]. On the triplet side, we recognize the narrow zero-bias resonance of the spin-1 Kondo effect with a small Kondo temperature $T_{K,1}$. As the singlet–triplet splitting decreases on either side, the anomalous finite-bias features previously discussed

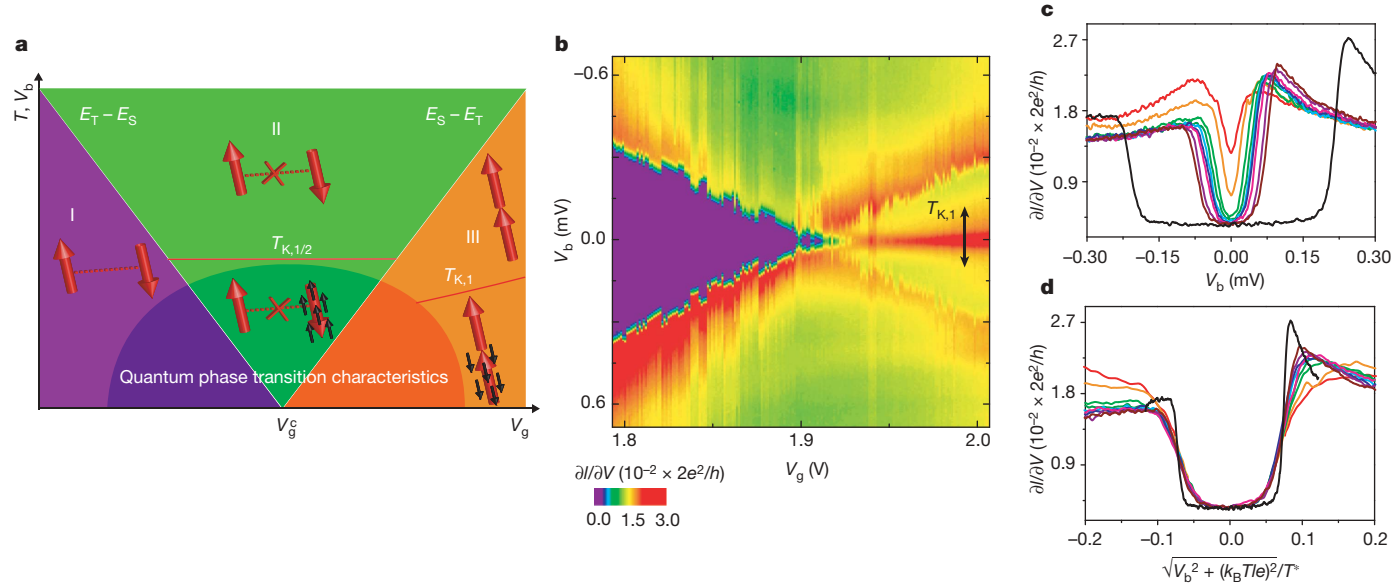

Figure 3 | Singlet–triplet quantum phase transition and universal scaling. **a**, Phase diagram as a function of V_g and V_b (or T): we identify regions according to whether V_b (or T) lies above the singlet–triplet splitting $|E_T - E_S|$. The effective spin states of the quantum dot are represented by large red arrows and screening electrons are represented by smaller, black arrows. The dotted line between the spins in region I indicates a strongly bound singlet state. In region II the two spin states decouple from each other (indicated by a crossed-out dotted line), and the spin that is more strongly coupled to the leads is fully screened by means of a spin-1/2 Kondo effect associated with the large Kondo temperature $T_{K,1/2}$. In region III the ground state of the quantum dot is a spin-1 triplet and experiences incomplete screening associated with the Kondo temperature $T_{K,1}$. **b**, Colour map of the differential conductance $\partial I/\partial V$ as a function of V_b and V_g for $T = 35$ mK and $B = 0$ T, close to the singlet–triplet transition. **c**, Differential conductance for different values of $V_g < V_g^c$, close to (inverse Kondo effect exhibiting a resonant dip) and far from (U-shaped curve) the transition point. **d**, Scaling analysis of the data in **c**, with respect to the singlet binding energy $k_B T^*$.

smoothly merge to form a broad resonance related to a second, much larger, Kondo temperature $T_{K,1/2}$. Theoretical calculations[2] indicate that the physics of the critical point can be described in terms of one molecular level undergoing a standard spin-1/2 Kondo effect while the remaining spin-1/2 unit in the dot remains decoupled from the electrodes (as long as a second screening channel can be neglected).

The phase diagram in Fig. 3a depicts the proposed model of the singlet–triplet phase transition. By examining the temperature dependence of the conductance in the different regions shown in this plot, we can gain valuable insights into the interpretation in terms of a Kosterlitz–Thouless transition. In region I of Fig. 3a we identify two different regimes. Far from the transition point, that is, when the splitting $E_T - E_S$ exceeds the Kondo energy $k_B T_{K,1/2}$, where $T_{K,1/2}$ is the spin-1/2 Kondo temperature and k_B denotes Boltzmann's constant, the two spins strongly bind into an interorbital singlet. The differential conductance thus exhibits a characteristic 'U'-shape as a function of source–drain voltage (which is associated with the singlet–triplet gap), as shown by the wide curve in Fig. 3c. Close to the transition point, $E_T - E_S$ becomes less than $k_B T_{K,1/2}$, so Kondo screening of one of the orbital levels occurs before the freezing of the interorbital singlet. This results in both a broad resonance in the associated differential conductance (Fig. 4c) and a logarithmic increase in temperature of the zero-bias data (Fig. 4d). This logarithmic increase can be accurately fitted to the empirical formula[26] extracted from the numerical-renormalization-group calculations[27]

$$G(T) = G_0\left(\frac{T^2}{T_{K,1/2}^2}\left(2^{1/s}-1\right)+1\right)^{-s} + G_c \qquad (1)$$

where G_0 is the conductance at $T = 0$, G_c is a fixed background conductance and $s = 0.22$, giving $T_{K,1/2} = 4.13 \pm 0.3$ K.

Following further cooling, an interorbital singlet forms between the remaining unpaired spin and the first orbital level, which now is part of the Fermi sea due to its hybridization with the conduction electrons during the first stage of Kondo screening. The decrease in the zero-bias conductance is thus associated with a second-stage Kondo effect between these new degrees of freedom, as shown (Fig. 4c) by the formation below 600 mK of a characteristic narrow Kondo dip inside the broad resonance of width $T_{K,1/2}$. This interpretation is supported by the decrease in the zero-bias conductance (Fig. 4d), which is described in terms of an inverted Kondo peak, as the second-stage Kondo effect upon further cooling is associated with a re-entrant Kondo effect, by the formula

$$G(T) = G_0\left(1-\left(\frac{T^2}{T^{*2}}\left(2^{1/s}-1\right)+1\right)^{-s}\right) + G_c \qquad (2)$$

where now G_0 is a typical conductance value, giving the renormalized singlet binding energy $k_B T^*$ with $T^* = 187 \pm 21$ mK.

Because the formation of the singlet state close to the transition point is associated with a re-entrant Kondo effect, we should expect universal behaviour of the conductance dip with a characteristic temperature T^*. Figure 3c shows that, at the base temperature $T = 35$ mK and for $V_g < V_g^c$, the differential conductance evolves from a Kondo-like lorentzian shape to a U shape. These data are shown rescaled[28] as a function of $\sqrt{V_b^2 + (k_B T/e)^2}/T^*$, where e is the electron charge, in Fig. 3d. This plot shows that the conductance curves coincide when studied close to the transition point, but that the scaling deteriorates as the singlet–triplet gap $E_T - E_S$ becomes

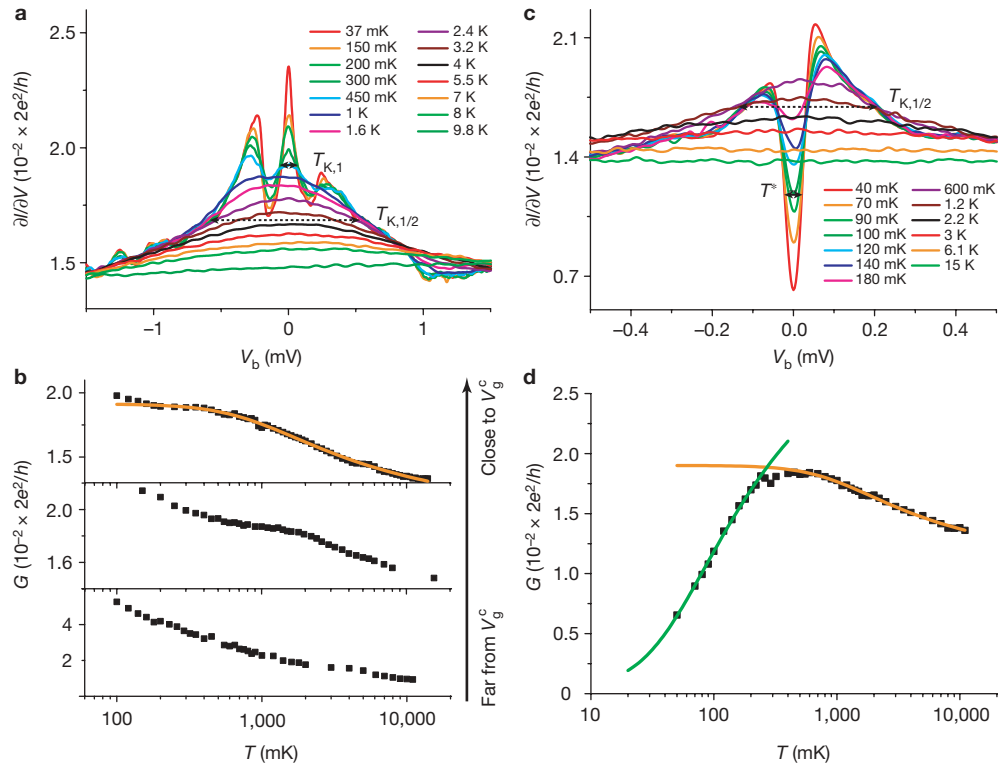

Figure 4 | Kondo effects in the singlet and triplet states. a, Differential conductance close to the transition point on the triplet side at different temperatures, showing a broad resonance with Kondo temperature $T_{K,1/2}$ and Kondo satellite peaks centred at $\pm|E_S - E_T|$. **b**, Temperature dependence of the zero-bias conductance $G(T)$ for three V_g values in the triplet region, the middle curve corresponding to **a**. We clearly measure a gate-dependent plateau, corresponding to the energy scale $|E_T - E_S|$. The solid line is a fit to equation (1), giving $T_{K,1/2} = 3.77 \pm 0.1$ K. The bottom panel, which does not show a clear plateau, corresponds to the temperature evolution of $G(T)$ in the underscreened spin-1 regime. **c**, Differential conductance close to the transition point on the singlet side at different temperatures, showing a broad resonance with Kondo temperature $T_{K,1/2}$ and a narrow dip (inverse Kondo effect) associated with a temperature scale T^*. **d**, Temperature dependence of the zero-bias conductance $G(T)$ corresponding to **c**. The orange line is a fit to equation (1), giving $T_{K,1/2} = 4.13 \pm 0.3$ K, and the green line is a fit to equation (2), giving $T^* = 187 \pm 21$ mK.

greater than $k_B T_{K,1/2}$. Our study of the temperature dependence of $G(T)$ and the scaling of $\partial I/\partial V$ with V_g, both on the singlet side of the transition, thus provides strong evidence for a Kosterlitz–Thouless-like transition.

We now turn to region III in Fig. 3a, where the triplet state is favoured over the singlet state. Far from the transition point, at large values of V_g, the spins are tightly bound into a triplet and we expect to observe an underscreened spin-1 Kondo effect. Estimates made from both the width of the zero-bias peak and its magnetic field splitting (not shown) converge to a Kondo scale $T_{K,1}$ of the order of 100 mK. This value is too low to allow quantitative comparison with theoretical predictions of the underscreened Kondo effect, but the conductance data plotted in the bottom panel in Fig. 4b do not show any sign of saturation down to our effective electronic temperature $T_{eff} = 50$ mK.

For lower gate voltages, a complex regime in which the singlet–triplet splitting $E_S - E_T$ is comparable to the high-energy, single-level Kondo scale $T_{K,1/2}$ exists. This is shown, for fixed V_g and a range of temperatures, by the differential conductance data plotted in Fig. 4a. Although a broad peak is again observed at high temperatures, a three-peak structure emerges at low temperatures. We interpret the three-peak structure in terms of a non-equilibrium Kondo effect that mixes singlet and triplet states by means of the voltage-bias window. We associate the broad peak with a spin-1/2 Kondo effect, similar to that which occurs on the singlet side, in agreement with the corresponding zero-bias conductance $G(T)$ for temperatures above the singlet–triplet splitting temperature, giving $T_{K,1/2} = 3.77 \pm 0.1$ K (top panel in Fig. 4b). This spin-1/2 Kondo behaviour remains similar down to the lowest temperatures by approaching the critical point, as $E_S - E_T$ becomes smaller than $k_B T_{K,1/2}$. The further increase of $G(T)$ below $T = 200$ mK is at present not fully understood, and may be related to the opening of a second screening channel, which might spoil the quantum critical point at $T = 0$ K[23,29]. However, this extra feature seems to be relevant only at a very small energy scale close to the crossing point, so the data in the accessible temperature range is consistent within the quantum critical point interpretation.

We finally note that our interpretation of the experimental data can be supported in a complementary way (see Supplementary Information), namely plotting the zero-bias conductance as a function of gate voltage for different temperatures. As the temperature decreases, we observe the clear sharpening of a conductance step when the system crosses from the singlet region to the triplet region, in agreement with the existence of a quantum critical point[3] and in contrast to the maximum predicted for an avoided transition[23,29].

METHODS SUMMARY

The single-molecule transistors were produced using standard electron-beam lithography to pattern a gold nanowire deposited on an Al/Al_2O_3 back gate; see Fig. 1b for an atomic-force-microscope micrograph with a diagram of the set-up. The nanowire junctions were cleaned with acetone, ethanol, isopropanol solution and oxygen plasma. Then a dilute toluene solution of C_{60} molecules was deposited on the junctions and blow-dried. The connected samples were placed in a copper shielded box that had high-frequency low-temperature filters. The box was anchored to the mixing chamber of the dilution fridge with a base temperature of 35 mK. The nanowire coated with molecules was then broken by electromigration[16] at 4 K, using fast real-time electronics to control the coupling of the single molecule to the electrodes.

Full Methods and any associated references are available in the online version of the paper at www.nature.com/nature.

Received 4 December 2007; accepted 18 March 2008.

1. Sachdev, S. Quantum magnetism and criticality. *Nature Phys.* **4,** 173–185 (2008).
2. Vojta, M., Bulla, R. & Hofstetter, W. Quantum phase transitions in models of coupled magnetic impurities. *Phys. Rev. B* **65,** 140405 (2002).
3. Hofstetter, W. & Schoeller, H. Quantum phase transition in a multilevel dot. *Phys. Rev. Lett.* **88,** 016803 (2002).
4. Sasaki, S. *et al.* Kondo effect in an integer-spin quantum dot. *Nature* **405,** 764–767 (2000).
5. Nygård, J., Cobden, D. H. & Lindelof, P. E. Kondo physics in carbon nanotubes. *Nature* **408,** 342–346 (2000).
6. Bogani, L. & Wernsdorfer, W. Molecular spintronics using single-molecule magnets. *Nature Mater.* **7,** 179–186 (2008).
7. Hewson, A. C. *The Kondo Problem to Heavy Fermions* (Cambrige Univ. Press, Cambridge, UK, 1993).
8. Glazman, L. I. & Raikh, M. E. Resonant Kondo transparency of a barrier with quasilocal impurity states. *JETP Lett.* **47,** 452–455 (1988).
9. Goldhaber-Gordon, D. *et al.* Kondo effect in a single-electron transistor. *Nature* **391,** 156–159 (1998).
10. Cronenwett, S. M., Oosterkamp, T. H. & Kouwenhoven, L. P. A tunable Kondo effect in quantum dots. *Science* **281,** 540–544 (1998).
11. Georges, A. & Meir, Y. Electronic correlations in transport through coupled quantum dots. *Phys. Rev. Lett.* **82,** 3508–3511 (1999).
12. Jones, B. A., Varma, C. M. & Wilkins, J. W. Low-temperature properties of the two-impurity Kondo hamiltonian. *Phys. Rev. Lett.* **61,** 125–128 (1988).
13. Affleck, I., Ludwig, A. W. W. & Jones, B. A. Conformal-field-theory approach to the two-impurity Kondo problem: Comparison with numerical renormalization-group results. *Phys. Rev. B* **52,** 9528–9546 (1995).
14. Zarand, G., Chung, C.-H., Simon, P. & Vojta, M. Quantum criticality in a double-quantum-dot system. *Phys. Rev. Lett.* **97,** 166802 (2006).
15. Liang, W., Shores, M. P., Bockrath, M., Long, J. R. & Park, H. Kondo resonance in a single-molecule transistor. *Nature* **417,** 725–729 (2002).
16. Park, H., Lim, A. K. L., Alivisatos, A. P., Park, J. & McEuen, P. L. Fabrication of metallic electrodes with nanometer separation by electromigration. *Appl. Phys. Lett.* **75,** 301–303 (1999).
17. Park, H. *et al.* Nanomechanical oscillations in a single-C_{60} transistor. *Nature* **407,** 57–60 (2000).
18. Kogan, A., Granger, G., Kastner, M. A., Goldhaber-Gordon, D. & Shtrikman, H. Singlet-triplet transition in a single-electron transistor at zero magnetic field. *Phys. Rev. B* **67,** 113309 (2003).
19. Quay, C. H. L. *et al.* Magnetic field dependence of the spin-1/2 and spin-1 Kondo effects in a quantum dot. *Phys. Rev. B* **76,** 245311 (2007).
20. Holm, J. V. *et al.* Gate-dependent tunneling-induced level shifts in carbon nanotube quantum dots. Preprint at ⟨http://aps.arxiv.org/abs/0711.4913⟩ (2007).
21. Paaske, J. *et al.* Non-equilibrium singlet-triplet Kondo effect in carbon nanotubes. *Nature Phys.* **2,** 460–464 (2006).
22. Nozières, P. & Blandin, A. Kondo effect in real metals. *J. Phys. (Paris)* **41,** 193–211 (1980).
23. Pustilnik, M. & Glazman, L. I. Kondo effect induced by a magnetic field. *Phys. Rev. B* **64,** 045328 (2001).
24. Pustilnik, M., Avishai, Y. & Kikoin, K. Quantum dot with even number of electrons: Kondo effect in a finite magnetic field. *Phys. Rev. Lett.* **84,** 1756–1759 (2000).
25. Craig, N. J. *et al.* Tunable nonlocal spin control in a coupled-quantum dot system. *Science* **304,** 565–567 (2004).
26. Grobis, M., Rau, I. G., Potok, R. M. & Goldhaber-Gordon, D. Kondo effect in mesoscopic quantum dots, in *Handbook of Magnetism and Magnetic Materials* Vol. 1 (eds Kronmüller, H. & Parkin, S.) Part II (Wiley, Chichester, 2007).
27. Costi, T. A. Kondo effect in a magnetic field and the magnetoresistivity of Kondo alloys. *Phys. Rev. Lett.* **85,** 1504–1507 (2000).
28. Potok, R. M., Rau, I. G., Shtrikman, H., Oreg, Y. & Goldhaber-Gordon, D. Observation of the two-channel Kondo effect. *Nature* **446,** 167–171 (2006).
29. Hofstetter, W. & Zarand, G. Singlet-triplet transition in lateral quantum dots: A numerical renormalization group study. *Phys. Rev. B* **69,** 235301 (2004).

Supplementary Information is linked to the online version of the paper at www.nature.com/nature.

Acknowledgements We acknowledge E. Eyraud and D. Lepoittevin for discussions and technical contributions regarding electronics and dilutions. We thank E. Bonet, T. Crozes and T. Fournier for lithography development, and C. Winkelmann, T. Costi and L. Calvet for discussions. The sample used in the investigations was made in the NANOFAB facility of the Néel Institut. This work is partially financed by ANR-PNANO, Contract MolSpintronics.

Author Information Reprints and permissions information is available at www.nature.com/reprints. Correspondence and requests for materials should be addressed to F.B. (franck.balestro@grenoble.cnrs.fr).

METHODS

The spin-1/2 Kondo effect in a C_{60} molecular junction was observed for the first time by Yu and Natelson[30] (see also the case of ferromagnetic electrodes[31]), and more recently by Parks *et al.*[32] using mechanically controllable break junctions. Although improvements of the original electromigration procedure[16] have also been reported recently[33–39], to our knowledge no electromigration has been carried out in a dilution refrigerator with a high degree of filtering. Because the creation of nanogaps using the electromigration technique requires minimizing the series resistance[39], the resistive dilution fridge wiring and filtering are generally incompatible with electromigration. However, accessing very low electronic temperatures is central to the observation of quantum critical signatures associated with the singlet–triplet crossing in the C_{60} molecular junction. To overcome this problem, we developed a specific electromigration set-up accessing very low electronic temperatures.

Our experimental method is divided into two parts (see Supplementary Fig. 1). In the first step, electromigration is performed at 4 K with the fast electronics of the set-up. We ramp the voltage across the junction and measure its resistance, using a very fast feedback loop (1.5 μs) to set the voltage to zero when the resistance exceeds a defined threshold, typically 20 kΩ. The fast feedback was achieved using an ADwin-Pro II real-time data acquisition system and a home-built high-bandwidth current-to-voltage converter. With this technique, and a series resistance due to the filters of about 200 Ω, we obtained small gaps (1–2 nm), which we characterized in terms of the tunnel current measured after electromigration of junctions without molecules.

The second step uses the low-noise component of the set-up to measure the single-molecule transistor. In addition to low-temperature filtering using a thermocoax microwave filter and Π filters, we used Π filters and ferrite-bead filters of special design with a cutoff frequency of 100 MHz (the details of these filters can be found at http://marcuslab.harvard.edu/how_to/Ferrite_Bead_Filter.pdf). To minimise ground loops we integrated all the analogue electronics in a shielded box at room temperature. Because of its great versatility, the ADwin-Pro II system can be programmed to perform direct-current and lock-in measurements, and apply gate or bias voltages, thus minimizing the possibility of ground loops. Depending on the measurements, we used an alternating-current excitation between 3 μV and 100 μV for the lock-in technique.

We note that previous studies of C_{60} quantum dots did not require the use of a dilution refrigerator to investigate Kondo physics, because the relevant energy scales are typically an order of magnitude larger than in carbon nanotubes or semiconducting devices, providing large Kondo temperatures of several Kelvins. However, the study of single-molecule transistors using low-temperature techniques (previously reserved to two-dimensional electron gases) was crucial for observing the rich physics that takes place below the Kondo temperature at the singlet–triplet transition. Our low-temperature set-up also allowed a more precise investigation of the usual spin-1/2 Kondo effect in C_{60} (see Supplementary Information section 2).

30. Yu, L. H. & Natelson, D. The Kondo effect in C_{60} single-molecule transistors. *Nano Lett.* **4**, 79–83 (2004).
31. Pasupathy, A. N. *et al.* The Kondo effect in the presence of ferromagnetism. *Science* **306**, 86–89 (2004).
32. Parks, J. J. *et al.* Tuning the Kondo effect with a mechanically controllable break junction. *Phys. Rev. Lett.* **99**, 026601 (2007).
33. Strachan, D. R. *et al.* Controlled fabrication of nanogaps in ambient environment for molecular electronics. *Appl. Phys. Lett.* **86**, 043109 (2005).
34. Houck, A. A., Labaziewicz, J., Chan, E. K., Folk, J. A. & Chuang, I. L. Kondo effect in electromigrated gold break junctions. *Nano Lett.* **5**, 1685–1688 (2005).
35. Esen, G. & Fuhrer, M. S. Temperature control of electromigration to form gold nanogap junctions. *Appl. Phys. Lett.* **87**, 263101 (2005).
36. Trouwborst, M. L., van der Molen, S. J. & van Wees, B. J. The role of Joule heating in the formation of nanogaps by electromigration. *J. Appl. Phys.* **99**, 114316 (2006).
37. O'Neill, K., Osorio, E. A. & van der Zant, H. S. J. Self-breaking in planar few-atom Au constrictions for nanometer-spaced electrodes. *Appl. Phys. Lett.* **90**, 133109 (2007).
38. Wu, Z. M. *et al.* Feedback controlled electromigration in four-terminal nanojunctions. *Appl. Phys. Lett.* **91**, 053118 (2007).
39. van der Zant, H. S. J. *et al.* Molecular three-terminal devices: fabrication and measurements. *Faraday Discuss.* **131**, 347–356 (2006).